Journal of Molecular Structure 1198 (2019) 126889

Contents lists available at ScienceDirect

Journal of Molecular Structure

journal homepage: http://www.elsevier.com/locate/molstruc

Synthesis of phosphine-containing novel Pd(II) and Ni(II) complexes: Electrochemical, photophysical and quantum chemical studies

Gurbet Yerlikaya [a, *], Eylül Büşra Tapanyiğit [a], Bilgehan Güzel [a], Onur Şahin [b], Gülfeza Kardaş [a]

[a] Çukurova University, Science and Letters Faculty, Chemistry Department, 01330, Adana, Turkey
[b] Sinop University, Scientific and Technological Research Application and Research Center, 57000, Sinop, Turkey

ARTICLE INFO

Article history:
Received 1 April 2019
Received in revised form
2 July 2019
Accepted 31 July 2019
Available online 5 August 2019

Keywords:
Bis(diphenylphosphinomethyl)aminobutyl
Electrochemistry
X-ray crystallography
Hartree Fock
Optical properties

ABSTRACT

Pd(II) and Ni(II) complexes of bis(diphenylphosphinemethyl) aminobutyl, $((Ph_2PCH_2)_2N(CH_2)_3(CH_3)_3)$, were synthesized using Schlenck techniques under nitrogen atmosphere. Synthesized complexes were characterized by using thermal analysis, elemental analyses, ^1H NMR, ^{31}P NMR, FT-IR and UV–Vis techniques. Single crystal X-Ray diffraction analysis confirms the structure of the newly synthesized compounds. The electrochemical properties of complexes were studied by using cyclic voltammetry. All complexes exhibited intra-ligand ($\pi \rightarrow \pi^*$) fluorescence in CH_2Cl_2. Hartree Fock was used to determine the electronic structure and properties of the complexes. Band gaps of the newly synthesized complexes were calculated as 3.19eV and 3.15eV and showed good optical properties.

1. Introduction

Phosphorus compounds are a group of very amazing ligands in organometallic chemistry, which are also helpful mediators in organic synthesis [1–4]. The synthesis of metal complexes carrying a phosphine ligand with usual stability and reactivity is yet one of the important research areas [5–7]. Like organometallic compounds, they give a range of electronic properties and a wide sort of structure adjusted by way of the coordinated metal center [8]. Metal complexes are likely to be formed from strong electron-donating phosphine group and coordinatively unstable phophonate group ligands [9]. Furthermore, phosphines of heteroleptic group 10 metal complexes have displayed amazing photoluminescent properties and molecular electrical conducting [10]. Also they have presented scarce C–H-M intramolecular interactions [11,12]. Resulting from the low-lying metal d-d excited states which allow nonradiative decay of the MLCT excited state, study concerning first row transition metals has been restricted because of their frequent intensely short-lived excited states compared to 2nd and 3rd row transition metal complexes [13–15]. Due to the d^{10} configuration of group 10 metal complexes, they exhibit longer excited-state existence [16]. According to the literature, studies on the photophysical properties and quantum chemical calculations of PCN type phosphines are very rare.

The purpose of this work was to synthesize Pd(II) and Ni(II) complexes of bis(diphenylphosphinomethyl)aminobutyl ligand. The compounds were identified together with single X-ray diffraction techniques and various spectroscopic techniques. Photophysical and electrochemical properties of the complex of Pd(II) and Ni(II) have also been studied. Theoretical calculations help to determine electronic structure and properties of complexes. It can be used to successfully relate the molecular structure, selectivity and chemical reactivity in the process, which further helps to understand the mechanism of a process on the molecular scale.

2. Experimental

2.1. Materials and methods

The synthesis was done under nitrogen atmosphere using Schlenk glassware. EtOH, Et_2O and CH_2Cl_2 were used as solvent. Solvents were dried using conventional techniques and freshly distilled under nitrogen atmosphere before use. Tetrabutyl ammoniumperchlorate (TBAP), $[PdCl_2(COD)]$(COD:1,5-

* Corresponding author.
E-mail address: gurbet.yerlikaya@gmail.com (G. Yerlikaya).

https://doi.org/10.1016/j.molstruc.2019.126889
0022-2860/

cyclooctadiene) and $NiCl_2$ were purchased from Sigma-Aldrich. The synthesis of bis(diphenylphosphinomethyl)aminobutyl were carried out according to literature procedures. Elemental analyses were studied using a Flash 2000 organic elemental analyzer. FT-IR spectra were obtained as KBr pellets in a 4000−450 cm^{-1} range with a PerkinElmer RX1 FT-IR system. UV−Vis spectra were taken using CH_2Cl_2 in a 200−800 cm^{-1} range with a PerkinElmer system. ^1H and ^{31}P, ^{13}C NMR spectra were taken at 25 °C in $CDCl_3$ with Varian Mercury 200 MHz NMR spectrometer. Luminescence properties were determined in dichloromethane (DCM) at room temperature with PerkinElmer LS 55 fluorescence spectrophotometer. Thermogravimetric curves were taken on a PerkinElmer Pyris Diamond TG/DTA at a heating rate of 10 °C/min under nitrogen atmosphere. Cyclic voltammetry measurements were carried out by using a Gamry interface 1000 electrochemical analyzer. Three-electrode configuration was used the cyclic voltammetry with Ag/AgCl electrode, glassy carbon electrode, and platinum wire as the reference, working, and auxiliary electrodes, respectively. 0.1M TBAP was used as the supporting electrolyte, in CH_2Cl_2.

2.2. Synthesis of bis(diphenylphosphinomethyl)aminobutyl $[(Ph_2PCH_2)_2N(CH_2)_3(CH_3)]$ ligand, (Dppab)

Phosphonium salt ($[Ph_2P(CH_2OH)_2]Cl$) (1.2 g, 4.26 mmol) was obtained using literature procedure [17] and dissolved in 2:1 H_2O/MeOH (60 mL). Triethylamine (Et_3N) (0.6 mL, 4.39 mmol) and n-butylamine (0.22 mL, 2.23 mmol) were added respectively to the solution of $[Ph_2P(CH_2OH)_2]Cl$) and stirred. The mixture was refluxed for 2 h, and then the oily product was extracted with CH_2Cl_2, and dried over $MgSO_4$. ^1H NMR ($CDCl_3$, ppm) δ: 7.49−7.69 (m, 20H, phenyl), 3.88 (d, $J = 3.2$ Hz, 4H, P-CH_2-N), 2.84 (t, $J = 7.6$ Hz, 2H, N-CH_2), 1.30 (m, 2H, N-CH_2**CH_2**CH_2CH_3), 1.21 (m, 2H, N-$(CH_2)_2$**CH_2**CH_3), 0.81 (t, $J = 7.2$ Hz, 3H, N-$(CH_2)_3CH_3$) ^{31}P NMR (DMSO-d_6, ppm) δ: −28.46.

2.3. Synthesis of Pd(II) complexes of Bis(diphenylphosphinomethyl)- aminobutyl $[PdCl_2(Ph_2PCH_2)_2N(CH_2)_3(CH_3)]$(1)

$PdCl_2$(COD) (0.41g, 1.46 mmol) in CH_2Cl_2 (10 mL) was added to a solution of $[(Ph_2PCH_2)_2N(CH_2)_3(CH_3)]$, (dppab), (0.69 g, 1.48 mmol) (Scheme 1.). The mixture was stirred for 3 h. The yellow solid formed at the end of the reaction. The product was filtered, washed with diethyl ether, and finally dried. X-ray quality crystals of the compounds were obtained by slowly evaporating in a CH_2Cl_2/Et_2O solution. Yield: 0.94 g, %98. FT-IR (KBr, cm^{-1}): 3053(Ar, C-H), 2927 (Aliphatic, C-H), 1626 (P- phenyl), 1437(P-C-N), 1307, 1198 (C-N-C), 737, 690 (monosubstituted, phenyl) (Fig. S1). ^1H NMR ($CDCl_3$, 25 °C) δ: 7.88−7.13 [m, 20H, 4phenyl], 3.39 [d, $J = 112$Hz., 4H, P-CH_2-N], 2.61 [t, $J = 72$ Hz, 2H, N-CH_2], 1.29 [m, 2H, N-CH_2**CH_2**CH_2CH_3], 1.04 [m, 2H, N$(CH_2)_2$**CH_2**CH_3], 0.77 [t, $J = 38.8$ Hz, 3H, N-$(CH_2)_3$**CH_3**)] (Fig. S2). ^{13}C NMR ($CDCl_3$, 25 °C) δ: 13.79 [P-CH_2-N-CH_2-CH_2-CH_2-**CH_3**], 20.27 [P-CH_2-N-CH_2-CH_2-**CH_2**], 27.55 [P-CH_2-N-CH_2-**CH_2**], 56.62 [P-CH_2-N-CH_2], 62.80 [P-CH_2-N], 128.58 [P-C-CH-CH-**CH,** phenyl], 129.27 [P-C-CH-**CH,** phenyl], 131.52 [P-C-**CH,** phenyl], 134.04 [P-C-CH, phenyl] (Fig. S3). ^{31}P NMR ($CDCl_3$, 25 °C) δ:7.99 ppm (Fig. S4). Anal. Calcd. for $C_{30}H_{33}Cl_2NP_2Pd$ (%) C, 55.66; H, 5.10; N, 2.17. Found (%): C, 55.46; H, 5.15; N, 2.08.

2.4. Synthesis of Ni (II) complexes of Bis(diphenylphosphinomethyl)-aminobuthyl $[NiCl_2(Ph_2PCH_2)_2N(CH_2)_3(CH_3)]$(2)

$NiCl_2$ (0.34g, 1.46 mmol) in CH_2Cl_2 (10 mL) was added to stirred solution of $[(Ph_2PCH_2)_2N(CH_2)_3(CH_3)]$, (dppab), (0.69g, 1.48 mmol) (Scheme 1). The mixture was stirred for 3 h and then solvent was evaporated. The compound was recrystallized in CH_2Cl_2/Et_2O. Yield: 0.79g, %90. FT-IR (KBr, cm^{-1}): 3054(Ar, C-H), 2955(Aliphatic, C-H), 1620(P-Ph), 1508, 1437 (P-C-N), 1307, 1194 (C-N-C), 736, 691(monosubstituted, Ph) (Fig. S5). ^1H NMR ($CDCl_3$, 25 °C) δ: 7.91−7.53 [m, 20H, 4phenyl], 3.37 [d, $J = 36$ Hz,4H, P-CH_2-N], 2.49[t, 2H, N-CH_2], 1.14[m, 2H, N-CH_2**CH_2**CH_2CH_3], 1.04 [m, 2H, N$(CH_2)_2$**CH_2**CH_3], 0.80 ppm[t, $J = 32$Hz., 3H, N-$(CH_2)_3$**CH_3**)(Fig. S6). ^{13}C NMR ($CDCl_3$, 25 °C) δ: 13.76 [P-CH_2-N-CH_2-CH_2-CH_2-**CH_3**], 20.03 [P-CH_2-N-CH_2-CH_2-**CH_2**], 27.75 [P-CH_2-N-CH_2-**CH_2**], 53.97 [P-CH_2-N-CH_2], 61.68 [P-CH_2-N], 128.62 [P-C-CH-CH-**CH,** phenyl], 131,82 [P-C-**CH,** phenyl], 137.16 [P-**C**-CH, phenyl] (Fig. S7). ^{31}P- NMR ($CDCl_3$, 25 °C) δ: 27.46 ppm (Fig. S8). Anal. Calcd. for $C_{30}H_{33}Cl_2NP_2Ni$ (%) C, 60.14; H, 5.55; N, 2.34. Found (%): C, 60.30; H, 5.75; N, 2.21.

^{31}P NMR data for ligand and metal complexes were given in Table 1.

2.5. X-ray diffraction analysis

Using a D8-QUEST diffractometer equipped with a graphite-monochromatic Mo-K_α radiation at 296 K for data collection, suitable crystals of 1−2 were chosen. Refining was done by full-matrix least-squares methods on F^2 with SHELXL-2013 [18] after the structures were solved by direct methods using SHELXS-97 [19]. All non-hydrogen atoms were purified with anisotropic parameters. The H atoms were identified from various maps and taken as treated as riding atoms with C-H distances 0.93−0.97 Å. In **1**-**2**, because the refine_diff_density max and min values are so small,

Table 1
^{31}P NMR data for ligand and metal complexes.

Compound	δ (ppm)	$\Delta\delta$(ppm)
$[(Ph_2PCH_2)_2N(CH_2)_3CH_3]$	−28.46	–
$[PdCl_2(Ph_2PCH_2)_2N(CH_2)_3CH_3]$	8.06	36.52
$[NiCl_2(Ph_2PCH_2)_2N(CH_2)_3CH_3]$	27.49	55.95

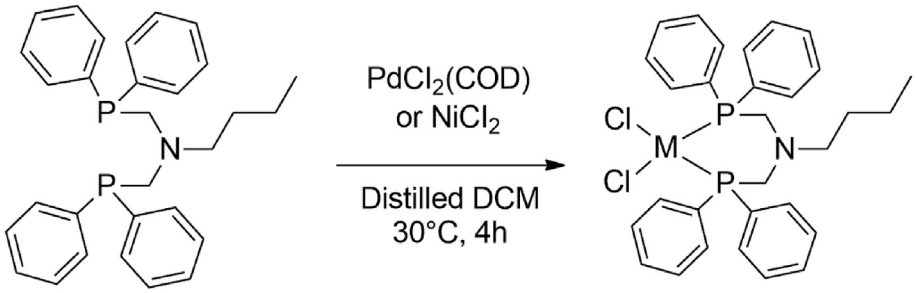

Scheme 1. Synthesis route of compounds of **1** and **2** (M: Pd, Ni).

the solvent molecules could not be located from Fourier map. For this reason, these molecules were eliminated from the refinement of the structure by means of the SQUEEZE subroutine of PLATON [20] and the hkl intensities were modified accordingly. The following procedures were used in our analysis: data collection: Bruker APEX2 [21]; program was used for molecular graphics were as follows: MERCURY programs [22]; software used to prepare material for publication: WinGX [23] Details of data collection and crystal structure determinations are given in Table 2.

2.6. Molecular structure evaluation

The structures of the complexes of 1 and 2 were investigated using Hartree Fock as applied in the Gaussian 09W program [24]. Avogadro software was made use of for geometry optimizations of the 1 and 2 molecule in the gas phase [25,26]. The geometries of the compounds were improved using Hartree Fock, method with a basis set of 3-21G for whole atoms lacking symmetry limits. The molecules were described using a Gaussian 09W package available with the Gaussian view 5.0 [27]. At a located constant point, the optimization was due to finish. Electronic properties of the 1 and 2 were looked into with electronegativity (χ), dipole moment (μ), global hardness (η), softness(S), energy of the highest occupied molecular orbital (E_{HOMO}), the lowest unoccupied molecular orbital (E_{LUMO}) and the energy gap (ΔE) between LUMO and HOMO.

3. Results and discussion

3.1. Characterization

The proton numbers calculated in the 1H NMR spectra were found to be consistent with the integration values. In the spectra, multiple substituted peaks of monosubstituted benzene are expected in the aryl-substituted phosphine compounds at about $\delta = 7.91–7.13$ ppm. The presence of doublets of $\delta = 3.37$ ppm showed peaks of the P-CH_2-N group [28,29]. Butyl peaks in the butylamine group were observed in the range of 0.80–0.77 ppm. According to ^{1}H NMR spectra, no remarkable difference was observed between the free phosphine ligand and metal complexes.

^{31}P NMR spectra of the complexes indicated more shielded signals than the dppab ligands, as shown in Table 1. The coordination shift values of the complexes (Δ), described by $\Delta = \delta$ (complex) $- \delta$ (free ligand), shift depending on the metal centers and the ligand itself (Table 1). On the basis of ^{31}P NMR data for the geometry of metal complexes, it has been suggested that these complexes have square planar geometry, as in those of notified studies [28,29].

Pd(ll) and Ni(ll) complexes were also characterized by FT-IR spectra. According to FT-IR spectra, the complexes indicate C–N–C stretching peaks around 1194–1198 cm^{-1} for tertiary amine. Aromatic C-H strecching band has been found at about 3053–3054 cm^{-1}; the peaks around 1620-1626 cm^{-1} and 690-737 cm^{-1} are assigned for monosubstitue benzene whereas bands in the range of 2927–2955 cm^{-1} are for aliphatic C-H streching.

Elemental analysis for C, H, N shows the basic formulas of the complexes. Based on analytical data, metal to ligan ratio has been found as 1:1 for complexes [30–32].

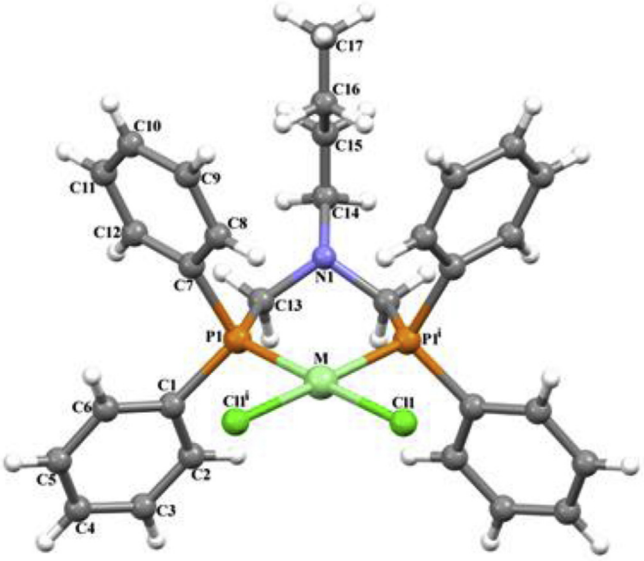

Fig. 1. The molecular structure of complexes **1-2** (M = Pd(II) in **1** and Ni(II) in **2**) showing the atom numbering scheme.

3.2. X-ray crystal structures of 1–2

The molecular structure of **1**–**2**, with the atom numbering scheme, is shown in Fig. 1. The crystallographic analyses show that

Table 2
Crystal data and structure refinement parameters for complexes **1-2**.

Crystal data	1	2
Empirical formula	$C_{30}H_{33}Cl_2NP_2Ni$	$C_{30}H_{33}Cl_2NP_2Pd$
Formula weight	599.12	646.81
Crystal system	Orthorhombic	Orthorhombic
Space group	Pnma	Pnma
a (Å)	21.961 (8)	21.956 (3)
b (Å)	17.533 (7)	17.853 (2)
c (Å)	8.032 (3)	8.0202 (8)
V (Å^3)	3093 (2)	3143.7 (6)
Z	4	4
D_c (g cm^{-3})	1.287	1.367
θ range (°)	2.9–24.8	2.9–26.0
μ (mm^{-1})	0.92	0.88
Measured refls.	22075	34600
Independent refls.	3133	3183
R_{int}	0.001	0.001
S	1.04	0.99
R1/w*R*2	0.052/0.124	0.053/0.121
$\Delta\rho_{max}/\Delta\rho_{min}$ (eÅ^{-3})	0.41/-0.31	1.09/-0.80

Table 3
Selected bond distances and angles for complexes **1-2** (Å, °).

	1	2
M-P1	2.1629(11)	2.2388(13)
M-Cl1	2.1999(11)	2.3558(13)
P1-M-P1^i	95.16(6)	94.46(7)
P1-M-Cl1	177.04(5)	177.46(5)
P1-M-Cl1^i	86.38(5)	87.13(5)

Symmetry code: (i) x, -y+1/2, z for **1**–**2** (M = Ni(II) in **1** and Pd(II) in **2**).

Table 4
The C-H···π interaction parameters for complexes **1-2** (Å, °).

D-H· · ·A	D-H	H···A	D···A	D-H···A
Complex 1				
C10—H10···Cg(1)^i	0.93	2.86	3.613 (5)	139
C12—H12···Cg(2)^{ii}	0.93	2.98	3.837 (4)	153
Complex 2				
C4—H4···Cg(1)^i	0.93	2.86	3.613 (7)	139

Symmetry codes: (i) 1/2-x, 1-y, −1/2 + z; (ii) 1/2-x, 1-y, 1/2 + z; Cg(1) = C1-C6; Cg(2) = C7-C12 for **1**; (i) 3/2-x, 1-y, 1/2 + z; Cg(1) = C7-C12 for **2**.

the complexes **1**-**2** appear very alike. Each complex crystallizes in the space group Pnma. Each M(ll) ion (M = Pd(ll) in **1** and Ni(ll) in **2**) is located on a center of symmetry and is coordinated by two chlorine atoms and two phosphorus atoms, thus displaying a square planar coordination geometry. The M-P bond distance is 2.1629(11) Å in **1** and 2.2388(13) Å in **2**, while the M-Cl bond distance is 2.1999(11) Å in **1** and 2.3558(13) Å in **2**, respectively. The bond angle of P-M-Pis 95.16(6)° in **1** and 94.46(7)° in **2** were given (Table 3). The molecules of **1**–**2** are linked by C-H … π interactions (Table 4). The joining of C-H···π interactions produce 2D supramolecular network running parallel to the *bc* plane in **1**–**2** (Fig. 2).

3.3. Thermal analyses

Thermal stability was found by TG/DTG studies from 50 to 900 °C for the complexes. The complexes were heated to 900 °C, all necessary weight loss was completed by 850 °C. TG/DTG curves drawn for phosphorus ligand [33] showed two endothermic mass loss stages. The TG/DTG curves of 1 shows two decomposition steps maximized at 320 and 700 °C (Fig. 3). The first clear peak at 250–400 °C coming with a mass loss matching to 72.875% (calculated. 72.59%) may be due to the release of dppab. The second decomposition stages at 400–850 °C involve the loss of Cl (observed = 9.195%, calculated = 10.976). The decomposition finished at 850 °C with Pd as a final residue (observed = 15.20%, calculated = 16.45%). The TG/DTG curves of 2 show two decomposition steps maximized at 300 and 600 °C (Fig. 4). The first clear peak at 150–350 °C is coming with a mass loss matching to 77.097% (calculated 77.85%) may be due to release of dppab. Other decomposition stages at 380–850 °C involve the loss of Cl (observed = 9.922%, calculated = 11.85). The decomposition finished at 850 °C with Ni as a final residue (observed = 11.00%, calculated = 9.80%).

3.4. Electronic properties

Absorption spectra of 1 and 2 were ascertained in CH_2Cl_2 solution (10^{-3} M) at room temperature (Fig. 5). Absorption spectra of

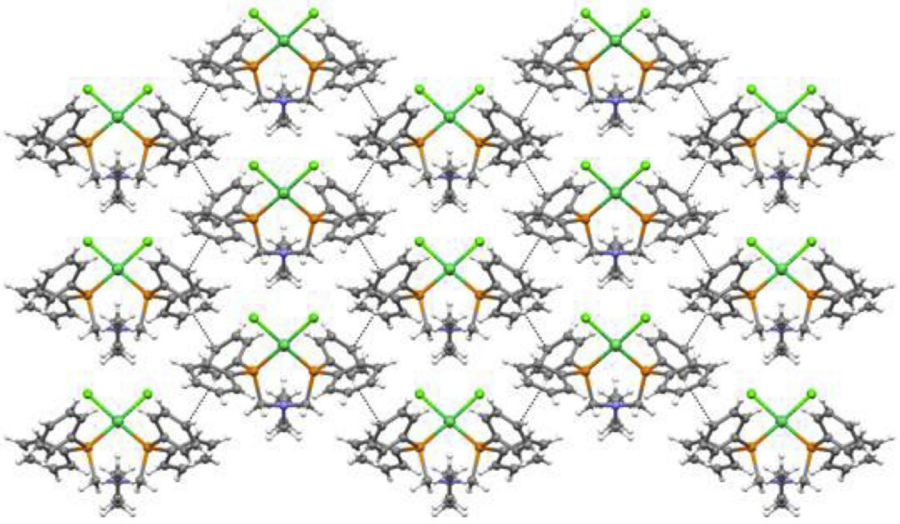

Fig. 2. The C-H···π interactions in **1**-**2**.

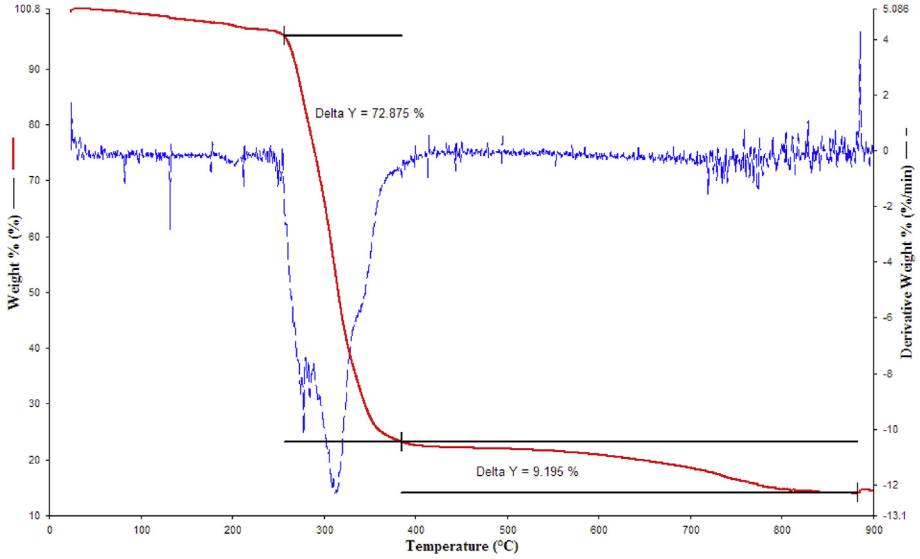

Fig. 3. TG and DTG curve of **1** complex.

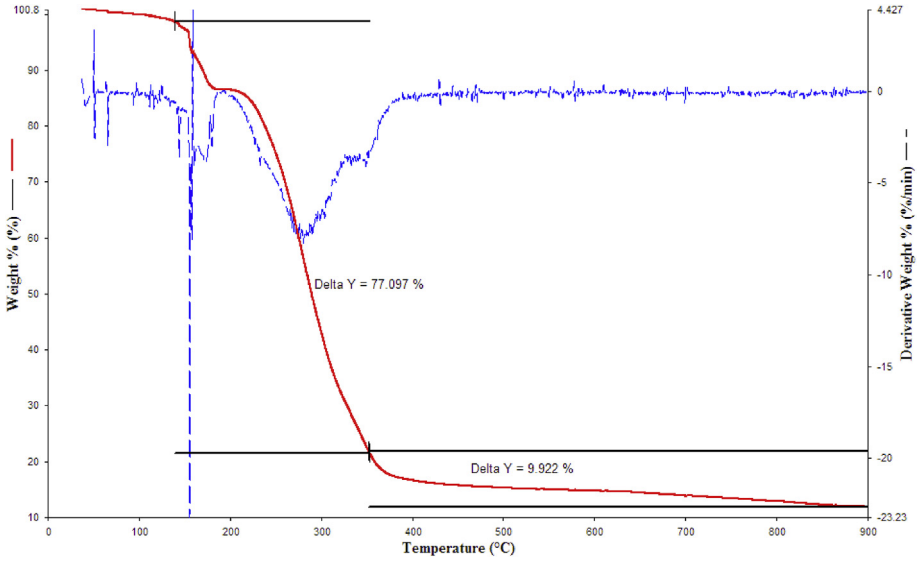

Fig. 4. TG and DTG curve of **2** complex.

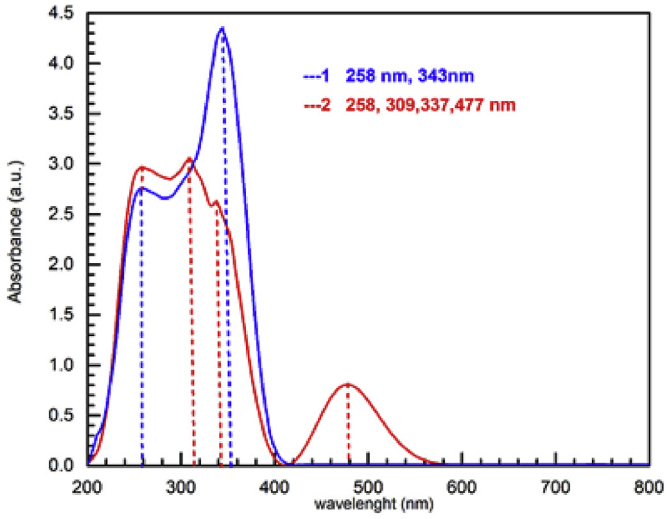

Fig. 5. UV–visible spectra of **1** and **2**.

Pd(ll) and Ni(ll) complexes show a strong absorption band at 258–309 nm for 1–2 which are tentatively designated as phosphine centered intra-ligand transition. Additionally to high-energy bands, a low-energy absorption band at 337–343 nm in 1–2 are likely designated as a mixture of intra-ligand ($\pi \rightarrow \pi^*$) transition with metal-ligand charge transfer (MLCT) transitions [34]. A weak absorption at around 477 nm in the spectra of 2 is designated to the spin allowed transition ($^1A_{1g} \rightarrow {}^1A_{2g}$) for four coordinate square planar geometry around Ni (ll).

3.5. Optical band gap analysis

UV spectral results were utilized to figure out the optical energy band gap of complexes 1 and 2. Optical energy band gap provides information about the use of complexes in photonic devices. Hence, it was calculated from equations (1) and (2).

The absorption coefficient (α) figure out according to the following relation:

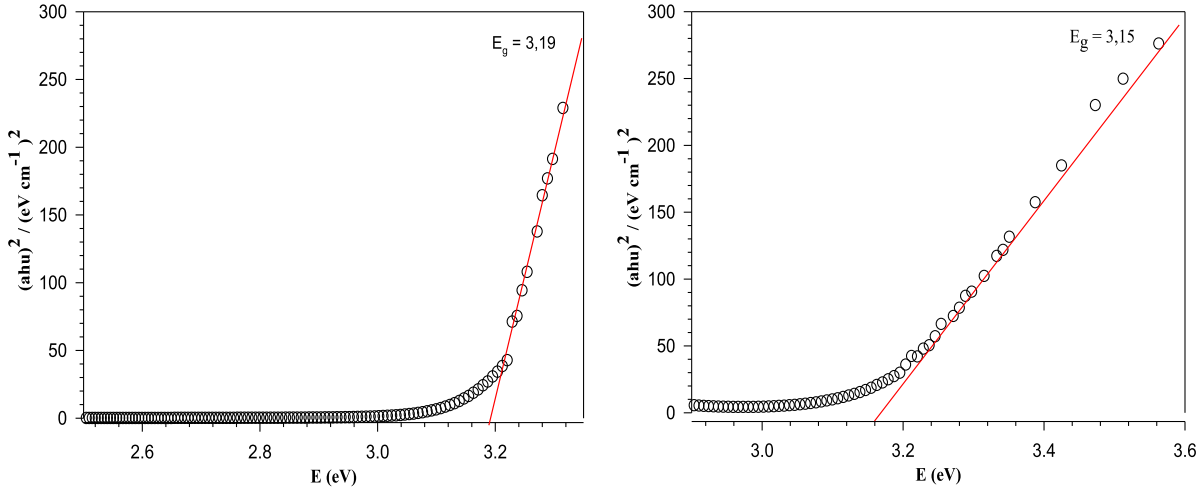

Fig. 6. Optical band gap spectra of complexes **1** (a), **2** (b).

$$\alpha = 2.303 \frac{Absorbance}{d} \quad (1)$$

where, d (= 1 cm) is the diameter of the tub. The Eg_{opt} was calculated with respect to the following equation [35–37].

$$(\alpha h\nu)1/r = A(h\nu - Eg) \quad (2)$$

where, the stationary such as h, A, ν are having their canonical senses, r is described as a sign value that discriminate the optical absorption continuum and the value of it for direct allowed transitions,1/2 [38–40]. The $(\alpha h\nu)^2$ vs hν, plots have been shown in Fig. 6 and the value of the optical energy band gap was carried from the point of interception on x(hν) axis where $(\alpha h\nu)^2 = 0$ and found to be 3.19 eV and 3.15eV, respectively. These values indicate that the compounds are within the visible region range.

3.6. Fluorescence spectral studies

The emission spectra of Pd(ll) (1) and Ni(ll) (2) complexes in CH_2Cl_2 at room temperature are illustrated in Fig. 7. The excitation of Pd (ll) and Ni (ll) complex in DCM solution resulted in emission at λ 557 nm and λ 583.5 nm, respectively. As shown in Fig. 7, the excitation intensity of Pd (II) complex is higher than that of Ni (II) complex. The emission peak observed in 1 and 2 was improved by a tune of 6.5 and 2.5 nm, respectively. Emission spectra also proved the formation of aminomethyldiphosphine metal complexes resulting to an increased energy gap between ground state and excited state. Emission spectra also prove an emission origin, mainly not only due to $\pi \rightarrow \pi^*$ intraligand transition but also with some metal-ligand charge transfer (MLCT) character [41,42].

3.7. Electrochemical properties of complexes 1 - 2

The electrochemical properties of complexes **1**–**2** were investigated cyclic voltammetry (CV). The CV's of 1 mM compounds 1, 2 and TBAP in 0.1 M TBAP under an inert atmosphere are shown in Fig. 8. The oxidation and reduction peaks of compounds **1**–**2** were observed at −0.760 V,-0.750V and at −0.960V, −0.950V, the onset potentials of oxidation and reduction of ferrocene were 0.298 V and 0.357 V (*vs.*Ag/AgCl) respectively.

The magnitude of ΔEp value gives information about irreversibility. When the ΔEp value increases, irreversibility increases. E_{HOMO}, E_{LUMO} and ΔE_g^{CV} are calculated according to equations

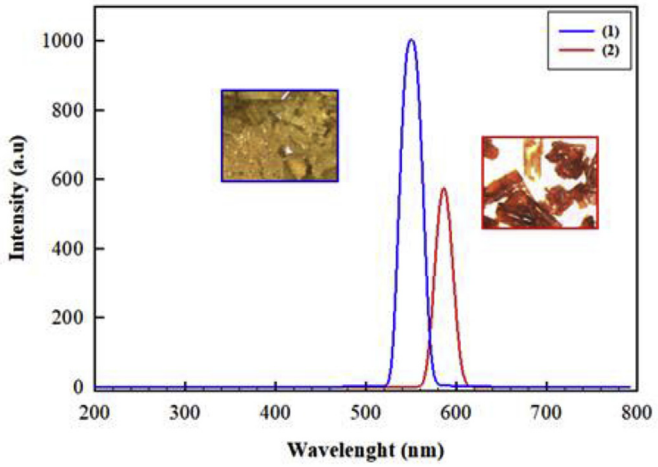

Fig. 7. The Emission spectra of **1** and **2**.

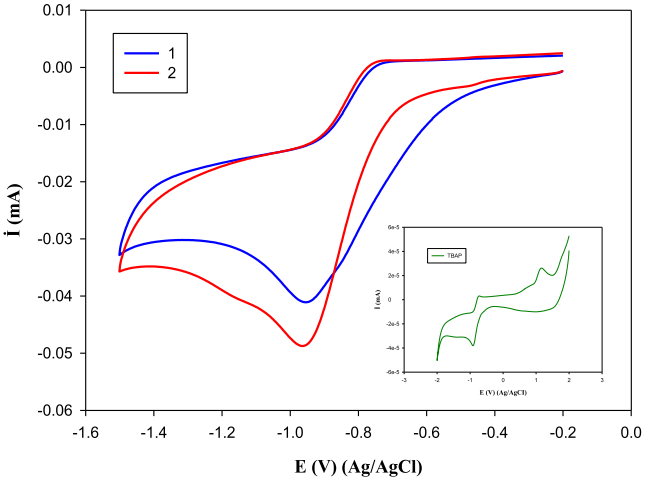

Fig. 8. The cyclic voltamogram of 1 mM (**1**, **2** complex and TBAP) at glassy carbon electrode in 0.1M TBAP + DCM solution at scan rate 100 mVs^{-1}.

(3)–(5) respectively.

$$EHOMO = [-e((Eoxonset(vs.\ Ag/AgCl) - (Eoxonset(Fc/Fc^+ vs.\ Ag/AgCl)) - 4.8eV] \quad (3)$$

$$ELUMO = [-e((Eredonset(vs.\ Ag/AgCl) - (Eredonset(Fc/Fc^+ vs.\ Ag/AgCl)) - 4.8eV] \quad (4)$$

$$\Delta EgCV = HOMO - LUMO \quad (5)$$

The electrochemical parameters listed in Table 5 were determined from CVs. The results obtained from Table 5 showed that the compounds were zero-valued and the minor ΔEp value indicated that the compounds were stable.

3.8. Theoretical calculations

Theoretical calculations help us understand the structure of **1** and **2**. The complexes were analyzed by working structure models (Figs. 9 and 10). Formation of the transition state linked to the interaction between E_{LUMO} and E_{HOMO} of reactants were found with the help of the molecular orbital theory [43]. The values of E_{HOMO} indicate the ability to donate electrons and emphasize the electron acceptor ability of molecular orbitals [44]. The size of E shows the stability of complexes of **1** and **2** [45]. Table 6 illustrates the corresponding E_{HOMO}, E_{LUMO}, ΔE, μ, χ, *S* and η values of the optimized structures of complexes of **1** and **2** [46]. For a molecule, the high ΔE means an electronic transition from the HOMO to the LUMO orbital and gives information about stability.

Also, the higher dipole moment is related to polarity and the dipole moments of the complexes of **1** and **2** are 16.18 and 27.94 Debye, respectively. According to these results, molecule **1** is more polar than molecule **2**.

$$\Delta E = E_{LUMO} - E_{HOMO} \quad (6)$$

Using equations (7)–(9) the quantum chemical parameters being the exact η, *S* and χ were calculated [45,47–49].

Table 5
Electrochemical parameters for **1**–**2** complexes (V).

Complexes	Epa	Epc	ΔEp	E_{HOMO}	E_{LUMO}	ΔEg^{CV}
$[PdCl_2(Ph_2PCH_2)_2N(CH_2)_3CH_3]$	−0.760	−0.960	0,200	−3.830	−3.190	−0.640
$[NiCl_2(Ph_2PCH_2)_2N(CH_2)_3CH_3]$	−0.750	−0.950	0.200	−3.820	−3.090	−0.730

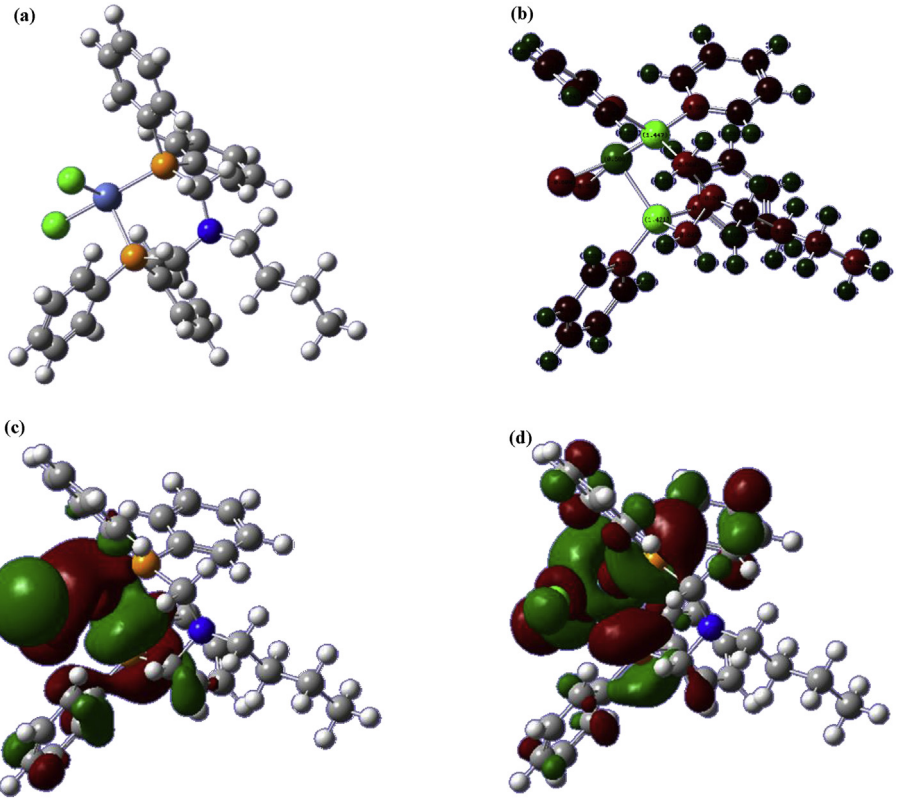

Fig. 9. Optimized structure **(a),** Mulliken charge (b), HOMO (c) and LUMO (d) for neutral compound **1**.

$$\chi = -\left(\frac{E_{LUMO} + E_{HOMO}}{2}\right) \quad (7)$$

$$\eta = \frac{E_{LUMO} - E_{HOMO}}{2} \quad (8)$$

$$S = \frac{1}{\eta} \quad (9)$$

These parameters provide information about the stability of molecules. Hard acids choose to react with hard base and likewise, soft acid selects a soft base according to hard, and soft acids and bases (HSAB) theory [50]. In the process, complexes of Pd and Ni behaved as a hard base. The results from Table 6 suggest that **2** is harder than **1**. Finally, χ indicates electron attracting ability of molecules. As formerly published [51], molecules with a rise in electronegativity tend to draw electrons from the metal.

4. Conclusions

Pd(II) and Ni(II) complexes with bis(diphenylphosphinomethyl) aminobutyl (PCN) ligand were prepared and characterized using spectroscopic techniques. The coordination of the (diphenylphosphinomethyl)aminobutyl ligand takes place via phosphorus atoms according to X-ray diffraction analyses and ^{31}P, ^{1}H NMR spectra. Cyclic voltamograms show that complexes display a reversible redox behavior matching to Pd(II)/Pd(0), Ni(II)/Ni(0) and TBAP. In addition, anodic and cathodic peak potentials and initial potentials of peaks were determined by voltamograms, ΔE values, HOMO-LUMO energies, band gap were calculated. The difference between HOMO-LUMO energy levels is very important in many respects. It gives insight into the stability of the structure, its optical properties, and in particular the electronic structure of matter. Complexes of 1 and 2 exhibit intra-ligand ($\pi \rightarrow \pi^*$) fluorescence in CH_2Cl_2. The emission spectrum and optical band gap calculated from UV–Vis spectrum. According to these results; The lowest optical band gap was observed in the compound Pd (II). Therefore,

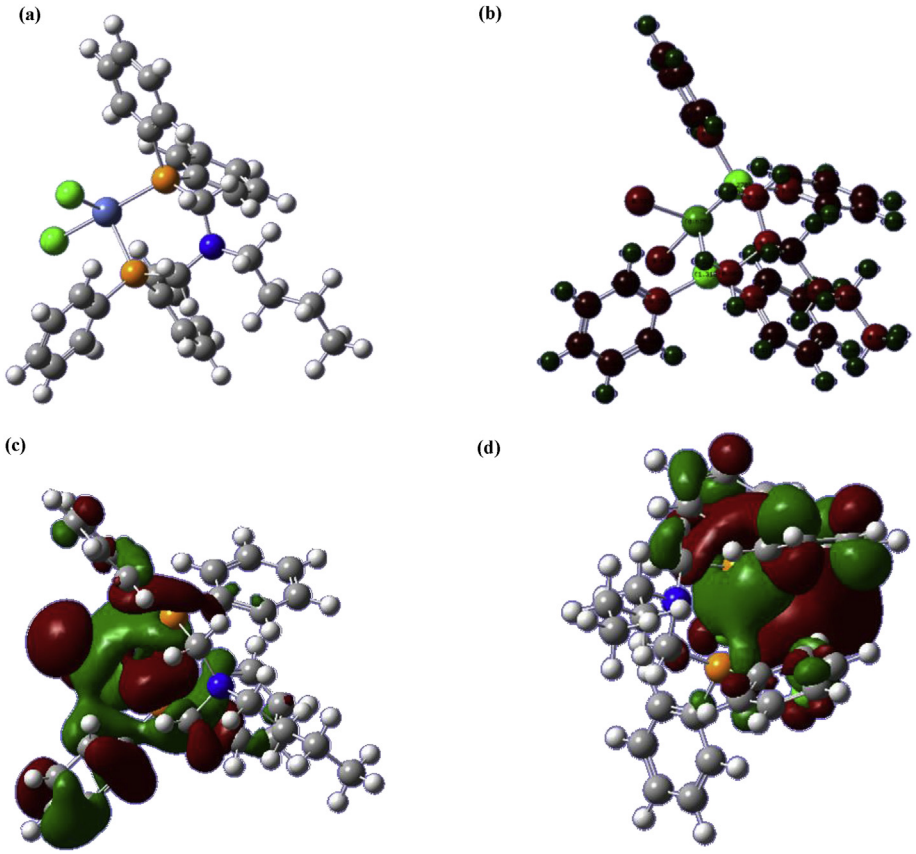

Fig. 10. Optimized structure **(a),** Mulliken charge (b), HOMO (c) and LUMO (d) for neutral compound **2**.

Table 6
The quantum chemical parameters of **1**–**2** complexes.

Complexes	E_{HOMO} (eV)	E_{LUMO} (eV)	ΔE (eV)	χ	η	S	μ
1	−7.04	+1.08	+8.12	+2.98	+4.06	+0.25	+15.06
2	−7.94	+2.07	+10.01	+2.94	+5.01	+0.20	+13.04

lower energy is needed to stimulate the Pd (II) complex and it has been found that Pd (II) compounds exhibit better photophysical properties than Ni (II) compounds for optical applications. From the theoretical calculations, as shown in Figs. 9 and 10 HOMO and LUMO nodes were generally delocalized on phenyl rings.

Acknowledgements

We thank Çukurova University for financial support (project no. FDK-2014-3517, FYL-2015-5201). We are grateful to Sinop University, The Scientific and Technological Research Application and Research Center, for the use of the Bruker D8 QUEST diffractometer.

Appendix ASupplementary data

Supplementary data to this article can be found online at https://doi.org/10.1016/j.molstruc.2019.126889.

References

[1] C.G. Kokotos, V.K. Aggarwal, Aminals as substrates for sulfur ylides: a synthesis of functionalized aziridines and -heterocycles, Org. Lett. 9 (11) (2007) 2099–2102.
[2] D. Janardanan, R.B. Sunoj, Computational investigations on the general reaction profile and diastereoselectivity in sulfur ylide promoted aziridination, Chemistry 13 (17) (2007) 4805–4815.
[3] O.I. Kolodiazhnyi, Methods of preparation of-substituted phosphorus ylides and their application in organic synthesis, Russ. Chem. Rev. 66 (3) (1997) 225–254.
[4] J. Heinicke, N. Peulecke, M. Köhler, M. He, W. Keim, Tuning of nickel 2-phosphinophenolates – catalysts for oligomerization and polymerization of ethylene, J. Organomet. Chem. 690 (10) (2005) 2449–2457.
[5] A. Vogler, H. Kunkely, Excited state properties of transition metal phosphine complexes, Coord. Chem. Rev. 230 (2002) 243–251.
[6] L. Dahlenburg, P-Modular bis(phosphines) based on the 1,2-trans-disubstituted cyclopentane framework in synthesis, coordination chemistry, and catalysis, Coord. Chem. Rev. 249 (24) (2005) 2962–2992.
[7] T.S. Lobana, P. Kumari, R. Sharma, A. Castineiras, R.J. Butcher, T. Akitsu, Y. Aritake, Thiosemicarbazone derivatives of nickel and copper: the unprecedented coordination of furan ring in octahedral nickel(II) and of triphenylphosphine in three-coordinate copper(I) complexes, Dalton Trans. 40 (13) (2011) 3219–3228.
[8] B.G. Bharate, A.N. Jadhav, S.S. Chavan, Synthesis, characterization, photoluminescence and optical properties of heterobimetallic Cu/Ru hybrid complexes composed of coordination and organometallic sites, Polyhedron 33 (1) (2012) 179–184.
[9] H.M.S. Bischoff, A. Weigt, B. Lticke, Soluble and supported carbonylation catalysts derived from rhodium-phosphonate-phosphane complexes, J. Mol. Catal. A Chem. 107 (1996) 339–346.
[10] D.D. Ellis, G. Harrison, A.G. Orpen, H. Phetmung, P.G. Pringle, J.G. deVries, H. Oevering, Platinum(II), palladium(II) and rhodium(I) complexes of o-, m- and p-Ph2PC6H4PO(OEt)2. PtCl2–SnCl2 Hydroformylation catalysts modified with phosphonated triarylphosphines, J. Chem. Soc., Dalton Trans. 5 (2000) 671–675.

[11] N. Singh, B. Singh, S.K. Singh, M.G.B. Drew, Syntheses, crystal structures and properties of sterically congested heteroleptic complexes of group 10 metal ions with p-tolylsulfonyl dithiocarbimate and 1,2-bis (diphenylphosphino) ethane, Inorg. Chem. Commun. 13 (12) (2010) 1451–1454.
[12] N. Singh, B. Singh, K. Thapliyal, M.G.B. Drew, Synthesis, X-ray crystal structures and properties of complex salts and sterically crowded heteroleptic complexes of group 10 metal ions with aromatic sulfonyl dithiocarbimates and triphenylphosphine ligand, Inorg. Chim. Acta 363 (13) (2010) 3589–3596.
[13] S. Ferrere, B.A. Gregg, Photosensitization of TiO2 by [FeII(2,2′-bipyridine-4,4′-dicarboxylic acid)2(CN)2]: band selective electron injection from ultra-short-lived excited states, Am. Chem. Soc. 120 (1998) 843–844.
[14] D.G.C. Shan-Ming Kuang, David R. McMillin, Phillip E. Fanwick, Richard A. Walton, Synthesis and structural characterization of Cu(I) and Ni(II) complexes that contain the bis[2-(diphenylphosphino)phenyl]ether ligand. Novel emission properties for the Cu(I) species, Inorg. Chem. 41 (2002) 3313–3322.
[15] C.L. Linfoot, P. Richardson, T.E. Hewat, O. Moudam, M.M. Forde, A. Collins, F. White, N. Robertson, Substituted [Cu(I)(POP)(bipyridyl)] and related complexes: synthesis, structure, properties and applications to dye-sensitised solar cells, Dalton Trans. 39 (38) (2010) 8945–8956.
[16] N. Robertson, CuI versus RuII: dye-sensitized solar cells and beyond, ChemSusChem 1 (12) (2008) 977–979.
[17] M. Keleş, O. Altan, O. Serindağ, Synthesis and characterization of bis(diphenylphosphinomethyl)amino ligands and their Ni(II), Pd(II) complexes: application to hydrogenation of styrene, Heteroat. Chem. 19 (2) (2008) 113–118.
[18] G.M. Sheldrick, Crystal structure refinement with SHELXL, Acta Crystallogr C Struct Chem 71 (Pt 1) (2015) 3–8.
[19] G.M. Sheldrick, A short history of SHELX, Acta Crystallogr. A 64 (Pt 1) (2008) 112–122.
[20] A.L.S. PLATON, A Multipurpose Crystallographic Tool, Utrecht, Utrecht University, The Netherlands, 2005.
[21] APEX2, Bruker, AXS Inc Madison Wisconsin USA, 2013.
[22] Mercury, version 3.3; CCDC, available online via ccdc.cam.ac.uk/products/mercury.
[23] L.J. Farrugıa, Computer program abstracts, J. Appl. Crystallogr. 32 (1999) 837–838.
[24] M. Frisch, G. Trucks, H. Schlegel, G. Scuseria, M. Robb, J. Cheeseman, G. Scalmani, V. Barone, B. Mennucci, G. Petersson, Gaussian 09 Revision D. 01, 2009, Gaussian Inc., Wallingford CT, 2009.
[25] M.D. Hanwell, D.E. Curtis, D.C. Lonie, T. Vandermeersch, G.R.H.E. Zurek, Avogadro: an advanced semantic chemical editor, visualization, and analysis platform, J. Cheminf. 4 (17) (2012).
[26] F. Tezcan, G. Yerlikaya, A. Mahmood, G. Kardaş, A novel thiophene Schiff base as an efficient corrosion inhibitor for mild steel in 1.0 M HCl: electrochemical and quantum chemical studies, J. Mol. Liq. 269 (2018) 398–406.
[27] R. Dennington, T. Keith, J. Millam, GaussView, Version 5, Semichem Inc., Shawnee Mission, KS, 2009.
[28] J. Fawcett, R.D. Kemmitt, D.R. Russell, O. Serindag, Zerovalent palladium and platinum complexes of aminomethylphosphines. Crystal structure of the palladium (0) dibenzylideneacetone complex [Pd (PhCH- CHCOCH- CHPh) {((C6H11) 2PCH2) 2NMe}], J. Organomet. Chem. 486 (1–2) (1995) 171–176.
[29] A.M. LaPointe, Parallel synthesis of aminomethylphosphine ligands, J. Comb. Chem. 1 (1) (1999) 101–104.
[30] M.J. McKeage, L. Maharaj, S.J. Berners-Price, Mechanisms of cytotoxicity and antitumor activity of gold (I) phosphine complexes: the possible role of mitochondria, Coord. Chem. Rev. 232 (1–2) (2002) 127–135.
[31] S.J. Berners-Price, R.J. Bowen, P. Galettis, P.C. Healy, M.J. McKeage, Structural and solution chemistry of gold (I) and silver (I) complexes of bidentate pyridyl phosphines: selective antitumour agents, Coord. Chem. Rev. 185 (1999) 823–836.
[32] J.S. Lewis, J. Zweit, P.J. Blower, Effect of ligand and solvent on chloride ion coordination in anti-tumour copper (I) diphosphine complexes: synthesis of [Cu (dppe) 2] Cl and analogous complexes (dppe= 1, 2-bis (diphenylphosphino) ethane), Polyhedron 17 (4) (1998) 513–517.
[33] S. Uruş, O. Serindağ, M. Diğrak, Synthesis, characterization, and antimicrobial activities of Cu(I), Ag(I), Au(I), and Co(II) complexes with [CH3N(CH2PPh2)2], Heteroat. Chem. 16 (6) (2005) 484–491.
[34] Ş. Güveli, N. Özdemir, A. Koca, T. Bal-Demirci, B. Ülküseven, Spectroscopic, electrochemical and X-ray diffraction studies on nickel(II)-complexes of acetophenone thiosemicarbazones substituted six-carbon groups, Inorg. Chim. Acta 443 (2016) 7–14.
[35] J. Tauc, R. Grigorovici, A. Vancu, Optical properties and electronic structure of amorphous germanium, Phys. Status Solidi 15 (2) (1966) 627–637.
[36] J. Tauc, Optical properties and electronic structure of amorphous Ge and Si, Mater. Res. Bull. 3 (1) (1968) 37–46.
[37] M. Shkir, H. Abbas, Z.R. Khan, Effect of thickness on the structural, optical and electrical properties of thermally evaporated PbI2 thin films, J. Phys. Chem. Solids 73 (11) (2012) 1309–1313.
[38] M. Shkir, S. Aarya, R. Singh, M. Arora, G. Bhagavannarayana, T. Senguttuvan, Synthesis of ZnTe nanoparticles by microwave irradiation technique, and their characterization, Nanosci. Nanotechnol. Lett. 4 (4) (2012) 405–408.
[39] F. Urbach, The long-wavelength edge of photographic sensitivity and of the electronic absorption of solids, Phys. Rev. 92 (5) (1953) 1324.
[40] M. Shakir, B. Singh, R. Gaur, B. Kumar, G. Bhagavannarayana, M. Wahab, Dielectric behaviour and ac electrical conductivity analysis of ZnSe chalcogenide nanoparticles, Chalcogenide Lett. 6 (12) (2009) 655–660.
[41] M. Shkir, P.S. Patil, M. Arora, S. AlFaify, H. Algarni, An experimental and theoretical study on a novel donor-pi-acceptor bridge type 2, 4, 5-trimethoxy-4'-chlorochalcone for optoelectronic applications: a dual approach, Spectrochim. Acta A Mol. Biomol. Spectrosc. 173 (2017) 445–456.
[42] D. Gudeika, V. Zilinskaite, J.V. Grazulevicius, R. Lytvyn, M. Rutkis, A. Tokmakov, 4-(Diethylamino)salicylaldehyde-based twin compounds as NLO-active materials, Dyes Pigments 134 (2016) 244–250.
[43] M. Finšgar, A. Lesar, A. Kokalj, I. Milošev, A comparative electrochemical and quantum chemical calculation study of BTAH and BTAOH as copper corrosion inhibitors in near neutral chloride solution, Electrochim. Acta 53 (28) (2008) 8287–8297.
[44] D. Daoud, T. Douadi, S. Issaadi, S. Chafaa, Adsorption and corrosion inhibition of new synthesized thiophene Schiff base on mild steel X52 in HCl and H2SO4 solutions, Corros. Sci. 79 (2014) 50–58.
[45] R.G. Pearson, Absolute electronegativity and hardness: application to inorganic chemistry, Inorg. Chem. 27 (4) (1988) 734–740.
[46] B. Xu, W. Yang, Y. Liu, X. Yin, W. Gong, Y. Chen, Experimental and theoretical evaluation of two pyridinecarboxaldehyde thiosemicarbazone compounds as corrosion inhibitors for mild steel in hydrochloric acid solution, Corros. Sci. 78 (2014) 260–268.
[47] O. Altan, O. Serindağ, K. Sayın, D. Karakaş, Pd (II) complexes of novel phosphine ligands: synthesis, characterization, and catalytic activities on Heck reaction, Phosphorus, Sulfur, Silicon Relat. Elem. 191 (7) (2016) 993–999.
[48] N. Karakus, K. Sayin, The investigation of corrosion inhibition efficiency on some benzaldehyde thiosemicarbazones and their thiole tautomers: computational study, J. Taiwan Inst. Chem. Eng. 48 (2015) 95–102.
[49] E. Arslan, A.A. Gürten, H.Z. Gök, M. Farsak, Electrochemical study of self-assembled aminothiol substituted phthalonitrile layers for corrosion protection of copper, ChemistrySelect 2 (27) (2017) 8256–8261.
[50] D. de la Fuente, I. Díaz, J. Simancas, B. Chico, M. Morcillo, Long-term atmospheric corrosion of mild steel, Corros. Sci. 53 (2) (2011) 604–617.
[51] A. Dutta, S.K. Saha, P. Banerjee, D. Sukul, Correlating electronic structure with corrosion inhibition potentiality of some bis-benzimidazole derivatives for mild steel in hydrochloric acid: combined experimental and theoretical studies, Corros. Sci. 98 (2015) 541–550.